ELECTRON PARAMAGNETIC RESONANCE OF THE Ti^{3+} ION IN $KAl(SO_4)_2 \cdot 12H_2O$

Michael A. Shannon

A THESIS

in

The Department

of

Physics

Presented in Partial Fulfillment of the Requirements

for the Degree of Master of Science at

Sir George Williams Campus

Concordia University

Montreal, Canada

April, 1975

Acknowledgements

The author wishes to express his gratitude to Dr. J.A. MacKinnon for proposing this topic and his constant aid and encouragement throughout the course of research.

A note of thanks is also extended to Mr. G.R. Sharp for many illuminating discussions and encouragement. The financial assistance provided by Dr. MacKinnon from his N.R.C. grant and by the Physics Department is greatly appreciated.

ABSTRACT

MICHAEL A. SHANNON

ELECTRON PARAMAGNETIC RESONANCE
OF THE Ti^{3+} ION IN $KAl(SO_4)_2 \cdot 12H_2O$

The electron paramagnetic resonance spectrum of Ti^{3+} ions in single crystals of $KAl(SO_4)_2 \cdot 12H_2O$ has been studied in the $\{100\}$ planes at 4.2^oK with an X-Band microwave spectrometer. The spectrum is an analogue of that reported by Dionne[3] for Ti^{3+} ions in $RbAl(SO_4)_2 \cdot 12H_2O$ and by MacKinnon and Dionne[10] for Ti^{3+} ions in $TlAl(SO_4) \cdot 12H_2O$.

The spectrum was explained by a model of 12 magnetic complexes being related to each other through the symmetry elements of the $T_h = (2/m)\bar{3}$ point group of the alum lattice.

The spin Hamiltonian used in the interpretation was $H_S = \beta g_{ij} H_i S_j$. The g-factors, with $S = \frac{1}{2}$ were found to be 1.979, 1.898 and 1.828 with an accuracy of $\pm$ .005.

TABLE OF CONTENTS

CHAPTER I

Introduction

Electron paramagnetic resonance, first seen by Zavoisky[19] in 1945, is basically concerned with the observation of transitions between the Zeeman levels when the paramagnetic substance is placed in a steady magnetic field and photons having energies equal to the gaps between the Zeeman levels irradiate the substance. Many classes of materials exhibit paramagnetism due to a resultant angular momentum possessed by the electrons. This resultant angular momentum may be due to many factors but two common reasons are: the atoms of the material have an odd number of electrons or there are ions present which possess partly filled electron shells as those which are found in the transition group.

The paramagnetic ion used in the author's experiments was a Ti^{3+} ion which belongs to the iron group, one of the sub-classes of the transition group. The free Ti^{3+} ion has a ground state of ^2D and only a single 3d electron which results in a spin of $\frac{1}{2}$ with only two populated Zeeman energy levels at liquid helium temperatures.

Single crystals of $KAl(SO_4)_2 \cdot 12H_2O$ doped with Ti^{3+} ions were grown by cooling to room temperature

a saturated solution of KAl alum plus titanium trichloride. In the crystals grown a small number of aluminum atoms are replaced in the lattice by ions of trivalent titanium.

Six H_2O molecules surround the Ti^{3+} ion forming a nearly regular octohedron which produces an electrostatic crystal field of orthorhombic symmetry. The spectrum obtained for the sample was explained with a model of 12 magnetic complexes and a crystal field of orthorhombic symmetry.

The technique used to observe the resonance involved the observation of the damping of a resonant circuit due to the energy absorbed by the sample from the applied r.f. field. The experiments were performed at X-Band frequencies using a Varian 4500 E.P.R. spectrometer.

CHAPTER II

THEORY

In order to understand how the lowest and excited energy levels of an ion situated in a crystal of given symmetry are altered by the crystalline surroundings it is first necessary to examine the situation for a free ion.

2.1 The General Hamiltonian of a Free Ion

The most important interaction within an ion is given by the coulomb term V_f. This term consists of the interaction of the electrons with the nuclear charge Ze and the mutual repulsion of the electrons. In the nonrelativistic approximation it is given by:

$$V_f = \sum_{k=1}^{N} \left(\frac{p_k^2}{2m} - \frac{Ze^2}{r_k} \right) + \sum_{k>j=1}^{N} \frac{e^2}{r_{kj}} \qquad (1)$$

where p_k is the linear momentum and r_k is the radius vector extending from the nucleus to the k^{th} electron and the whole expression is summed over all N electrons of the ion. This coulomb repulsion is different for different states of the same configuration and correspondingly leads to various energy levels or term values.

The next most important interaction is a magnetic one, V_{LS}, between the electron spins $\vec{s}_k$ with the orbital momentum $\vec{l}_k$. It is given by:

$$V_{LS} = \sum_{jk} a_{jk} \vec{l}_j \cdot \vec{s}_k + b_{jk} \vec{l}_j \cdot \vec{l}_k + c_{jk} \vec{s}_j \cdot \vec{s}_k \qquad (2)$$

where a_{jk}, b_{jk}, and c_{jk} are specific constants and j and k range over all electrons.

If Russell-Saunders coupling is assumed, that is, states of definite L and S of the same configuration, then $\sum \vec{l}_i = \vec{L}$ and $\sum \vec{s}_j = \vec{S}$ and the vectors $\vec{L}$ and $\vec{S}$ couple to give the total angular momentum $\vec{J} = \vec{L} + \vec{S}$ and the spin - orbit interaction can be written as[15] $\lambda \vec{L} \cdot \vec{S}$ where λ is the spin orbit constant for a given ion. There is also the much weaker spin - spin interaction V_{SS}, which is the mutual interaction between the magnetic dipoles and may be expressed as:

$$V_{ss} = \sum_{jk} \left\{ \frac{\vec{s}_j \cdot \vec{s}_k}{\mathcal{R}_{jk}^2} - \frac{3(\vec{\mathcal{R}}_{jk} \cdot \vec{s}_j)(\vec{\mathcal{R}}_{jk} \cdot \vec{s}_k)}{\mathcal{R}_{jk}^5} \right\} \qquad (3)$$

where the summation is extended over all pairs of electrons. The preceding three terms constitute the dominant forces within the free ion, but others need be considered.

If the nucleus has a spin I and a quadrupole moment Q, the various terms are again split by two additional interactions, V_N and V_Q where:

$$V_N = 2\gamma\beta\beta_N \left[\sum_k \left\{ \frac{(\vec{l}_k - \vec{s}_k)\cdot\vec{I}}{\Omega_k^3} + \frac{3(\vec{\Omega}_k\cdot\vec{s}_k)(\vec{\Omega}_k\cdot\vec{I})}{\Omega_k^5} \right\} + \frac{8\pi}{3}\delta(\vec{\Omega}_k)(\vec{s}_k\cdot\vec{I}) \right] \quad (4)$$

$$V_Q = \frac{e^2Q}{2I(2I-1)} \left\{ \sum_k \frac{I(I+1) - 3(\vec{\Omega}_k\cdot\vec{I})^2}{\Omega_k^3} \right\} \quad (5)$$

Here: s_k = Spin of electron k

l_k = Orbital angular momentum of electron k

β = Bohr magneton

β_N = Nuclear magneton

γ = Nuclear gyromagnetic ratio

δ = Dirac Delta function

If the ion is not free but is in the presence of a magnetic field the term V_H must be included in the Hamiltonian in order to describe its interaction with the field. This term is given by:

$$V_H = \sum_k \beta(\vec{l}_k + 2\vec{s}_k)\cdot\vec{H} \quad (6)$$

and the direct interaction of the nucleus with the field H is:

$$V_h = -\gamma\beta_N \vec{H}\cdot\vec{I} \quad (7)$$

The general Hamiltonian of an ion in an external magnetic field is given by the sum of all the above terms.

This Hamiltonian is:

$$\mathcal{H} = V_F + V_{LS} + V_{SS} + V_N + V_Q + V_H + V_h \qquad (8)$$

The approximate order of magnitude of these interactions can be estimated from the observed atomic spectra. $V_F = 10^5$ cm.$^{-1}$ and for the iron group $V_{LS} = 10^2$ cm.$^{-1}$; $V_{SS} =$ cm.$^{-1}$; $V_N = 10^{-1} - 10^{-3}$ cm.$^{-1}$ and $V_Q = 10^{-3}$ cm.$^{-1}$.

2.2 The Resonance Condition for a Free Ion

If a free ion with a resultant angular momentum J is placed in a magnetic field H, the energies[2] of the levels associated with different orientations are $g\beta HM$ where g is the spectroscopic splitting factor, β is the Bohr magneton and M is the component of the electric angular momentum J along the field acting on the ion. Also if an alternating field of frequency ν is applied at right angles to H, magnetic dipole transitions are produced according to the selection rule $\Delta M = \pm 1$. The magnetic field for a given frequency quantum may be described by:

$$h\nu = g\beta H \qquad (9)$$

Energy will be absorbed if the spin of the electron is flipped from a direction approximately parallel to the magnetic field to that of the approximately anti-parallel direction, that is, from a lower energy state to one of higher energy.

In most cases the distribution of electrons between the two states is governed by a Maxwell - Boltzmann expression which is:

$$\frac{N_1}{N_2} = \exp\left(-\frac{h\nu}{kT}\right) \qquad (10)$$

where N_2 is the number in the upper energy state and N_1 is the number in the lower energy state. T is the absolute temperature and k is the Boltzmann constant. The lower energy levels are more densely populated and for room temperature Eqn.(10) gives a ratio of approximately 0.995 at X - Band frequencies.

Because upward and downward transitions both have equal probabilities it is seen that the application of radiation will result in the tendency toward equality of the level populations which represents a net absorption of energy from the radiation field. Observation of this absorption is possible by placing the sample in a tuned circuit such as a cavity where absorption of energy is indicated when damping of the circuit occurs.

It may be seen from Eqn.(10) that it is highly advantageous to operate at as high a frequency and at as low a temperature as possible. The main reason for this is to maximize the difference between N_1 and N_2 which, at resonance, increases the net absorption of energy and thus optimizes the experimental sensitivity.

2.3 Effect of the Crystal Field Potential on the Paramagnetic Ion

In a previous section it was seen that Eqn.(8) was the complete Hamiltonian for a free ion but in practice we are not concerned with a free ion but an ion within the lattice structure of a specific crystal. It is, therefore, necessary to alter the free ion Hamiltonian in order to take into account the bound ion's surrounding environment.

The usual method to estimate the effect of the crystal in modifying magnetic properties is to adopt the concept of crystalline field approximation.[18] In this approximation the assumption must be made that the surrounding ions are point charges or point dipoles whose influence, on the paramagnetic ion, are exerted strictly by the electric field they produce at the ion's site. Another assumption must be made and that is that the surrounding ions are given a passive role and are regarded as point charges which do not overlap the paramagnetic ion.[12] Thus the electrostatic potential obeys Laplace's equations: $\nabla^2 V = 0$. A complete set of solutions for this equation are the generalized Legendre polynomials. It is possible to expand the potential in terms of these

polynomials with the result being:

$$V_x = \sum_{m} \sum_{m=-m}^{m} \sum_{k} A_m^m \beta^m Y_m^m(\theta_k, \varphi_k) = \sum_{m} \sum_{m} V_m^m \qquad (11)$$

where the summation K, is over all the electrons. This electrostatic interaction term V_x causes splitting of the order of 10^3 cm^{-1} or greater.

The complete Hamiltonian of a paramagnetic ion subject to a crystal field and in an external magnetic field is then given by:

$$\mathcal{H}_T = V_F + V_{LS} + V_{SS} + V_N + V_Q + V_H + V_h + V_X \qquad (12)$$

Since V_F, V_Q and V_h are spin independent and these terms do not contribute to the energy differences due to the fact that they shift all energy levels equally they may justifiably be deleted from Eqn.(12). The total electronic spin Hamiltonian for the ion under the influence of a crystalline environment and placed in a magnetic field may then be represented as:

$$\mathcal{H}_S = V_{LS} + V_{SS} + V_N + V_H + V_X \qquad (13)$$

2.4 The Spin Hamiltonian for Ti^{3+} In $KAl(SO_4)_2.12H_2O$

For a Ti^{3+} ion substituted in a single crystal of potassium aluminum sulphate dodecahydrate, which is a spin system of $\frac{1}{2}$, the spin Hamiltonian of Eqn. 12 reduces to:

$$\mathcal{H}_s = \sum_{\alpha,\beta=i}^{k} \beta g_{\alpha\beta} H_\alpha S_\beta \qquad (14)$$

where i, j and k are taken to be the axes of the cubic lattice.

Summing over the axes Eqn(14) may be written as:

$$\mathcal{H}_s = \beta\{g_{ii} H_i S_i + g_{jj} H_j S_j + g_{kk} H_k S_k + g_{ij} H_i S_j + g_{ji} H_j S_i + g_{ik} H_i S_k + g_{ki} H_k S_i + g_{jk} H_j S_k + g_{kj} H_k S_j\} \qquad (15)$$

By determining the complete matrix for the spin Hamiltonian and solving, the energy E is given by:

$$E = \pm\frac{\beta}{2}\{(g_{kk}H_k + g_{ik}H_i + g_{jk}H_j)^2 + (g_{ii}H_i + g_{ij}H_j + g_{ik}H_k)^2 + (g_{jj}H_j + g_{ij}H_i + g_{jk}H_k)^2\}^{1/2} \qquad (16)$$

The Zeeman energy splitting may now be expressed as:

$$\Delta E = |E_1 - E_2| = \beta\{(g_{kk}H_k + g_{ik}H_i + g_{jk}H_j)^2 + (g_{ii}H_i + g_{ij}H_j + g_{ik}H_k)^2 + (g_{jj}H_j + g_{ij}H_i + g_{jk}H_k)^2\}^{1/2} \qquad (17)$$

If the applied magnetic field H is in the (1,2) plane then H_3 may be set equal to zero and $H_1 = H\cos\Theta$ and $H_2 = H\sin\Theta$ and the Zeeman energy splitting becomes:

$$\Delta E = \beta H \left\{ (g_{i1}^2 + g_{i2}^2 + g_{ik}^2)\cos^2\Theta + (g_{i1}^2 + g_{i2}^2 + g_{ik}^2)\sin^2\Theta + (g_{ik}g_{ik} + g_{i1}g_{i2} + g_{i1}g_{i2})\sin 2\Theta \right\}^{1/2} \quad (18)$$

Now at the point of resonance, $\Delta E = h\nu$, which is the photon energy of the applied electromagnetic energy and by substituting into Eqn. (18) the expression for the magnetic field H_o at resonance in the (1,2) plane is:

$$H_o = \frac{h\nu}{\beta}\left\{ X\cos^2\Theta + Y\sin^2\Theta + Z\sin 2\Theta \right\}^{-1/2} \quad (19)$$

where: $X = (g_{i1}^2 + g_{i2}^2 + g_{ik}^2)$

$Y = (g_{i1}^2 + g_{i2}^2 + g_{ik}^2)$.

$Z = (g_{ik}g_{ik} + g_{i1}g_{i2} + g_{i1}g_{i2})$

2.5 Determination of the g_{ij} Tensors

By using calculations similar to those in the previous section the expressions for H_o in the (2,3) and (3,1) planes become respectively:

$$H_o = \frac{h\nu}{\beta}\left\{ (g_{i1}^2 + g_{i2}^2 + g_{ik}^2)\cos^2\Theta + (g_{k1}^2 + g_{k2}^2 + g_{ik}^2)\sin^2\Theta + (g_{k1}g_{ik} + g_{i1}g_{i2} + g_{i1}g_{ik})\sin 2\Theta \right\}^{-1/2} \quad (20)$$

and: $$H_0 = \frac{h\nu}{\beta}\left\{\left(g_{kk}^2 + g_{ik}^2 + g_{jk}^2\right)\cos^2\theta + \left(g_{ii}^2 + g_{ij}^2 + g_{ik}^2\right)\sin^2\theta + \left(g_{kk}g_{ik} + g_{ii}g_{ik} + g_{ij}g_{jk}\right)\sin 2\theta\right\}^{-1/2} \quad (21)$$

The preceding 3 equations give the value of the magnetic field at the point of resonance. By experimentally determining this value at various angles (0°, 45° and 90°) and using Eqn.19, 3 equations are produced which relate the six unknown g_{ij} tensor elements. In order to solve for these elements 3 more equations are required. These are arrived at by repeating the magnetic field determinations in the (2,3) and (3,1) planes and utilizing Eqns.(20) and (21). Once these six equations are arrived at a method of mathematical iteration is employed.

As an example the following six equations were obtained by the above technique:

$$\frac{h\nu}{H_0\beta} = \left\{g_{ii}^2 + g_{ij}^2 + g_{ik}^2\right\}^{1/2} = A^{1/2} \quad (22)$$

$$\frac{h\nu}{H_0\beta} = \left\{g_{jj}^2 + g_{ij}^2 + g_{jk}^2\right\}^{1/2} = B^{1/2} \quad (23)$$

$$\frac{h\nu}{H_0\beta} = \left\{g_{kk}^2 + g_{ik}^2 + g_{ik}^2\right\}^{1/2} = C^{1/2} \quad (24)$$

$$\frac{h\nu}{H_0\beta} = \left\{\frac{A}{2} + \frac{B}{2} + g_{ik}g_{ik} + g_{ii}g_{ij} + g_{ii}g_{ij}\right\}^{1/2} \quad (25)$$

$$\frac{h\nu}{H_0\beta} = \left\{\frac{B}{2} + \frac{C}{2} + g_{kk}g_{ik} + g_{ik}g_{ij} + g_{ii}g_{ik}\right\}^{1/2} \quad (26)$$

$$\frac{h\nu}{H_0\beta} = \left\{ \frac{C}{2} + \frac{A}{2} + g_{kk}g_{ik} + g_{ii}g_{ik} + g_{ij}g_{jk} \right\}^{1/2} \qquad (27)$$

By applying the iteration technique the solution of these equations is a symmetric tensor of the form:

$$\begin{pmatrix} g_{ii} & g_{ij} & g_{ik} \\ g_{ij} & g_{ii} & g_{ik} \\ g_{ik} & g_{ik} & g_{kk} \end{pmatrix} = \begin{pmatrix} 1.93678 & .02347 & .03002 \\ .02347 & 1.95327 & .04685 \\ .03002 & .04685 & 1.91729 \end{pmatrix}$$

which upon diagonalization yields the principle g values which were found to be $g_z = 1.979$, $g_x = 1.828$ and $g_y = 1.838$. The orientations of the 12 g_{ij} tensors along with their direction cosines are presented in Table 5.

CHAPTER III

CRYSTALLOGRAPHY

The alum is a hydrate belonging to the pyritohedral class of the cubic or isometric system. It is also a series of double[6] salts which may be classified chemically by the formula

$$R^{1+}R^{3+}(R^{6+}O_4)_2 \cdot 12H_2O$$

where: R^{1+} is a monovalent metal ion

R^{3+} is a trivalent metal ion

R^{6+} is Sulfur, Selenium or Tellurium

In the author's case: R^{1+} = Potassium (K)

R^{2+} = Aluminum (Al)

R^{6+} = Sulfur (S)

which when combined resulted in the crystal alum of potassium aluminum sulphate dodecahydrate: $KAl(SO_4)_2 \cdot 12H_2O$.

From a crystal structure standpoint the alums belong to the cubic system with 4 molecules in unit of edge length a_o = 12.158 Angstroms. More specifically they are of space group $T_h^6(Pa3)$ with point group symmetry of $T_h = \frac{2}{m}\bar{3}$, where the metal ions occupy alternate sites on the corners of the cube.[4] The positions and bonding arrangements for a typical α or β alum are shown in Figure 1.

In all known cases six water molecules are closely

coordinated with the small trivalent metal ions. Each of these trivalent metal ions has as its nearest neighbors six water molecules forming a nearly regular octohedron.

For a majority[17] of the alums, commonly designated as α alums and typified by $KAl(SO_4)_2.12H_2O$ the univalent cation is also surrounded by six octahedrally distributed water molecules. The distribution of these 6 water molecules depends mainly on the size of the monovalent ions used and to some extent characterizes the formation of α, β or γ types of alums. The formula for the potassium alum may also be written as $(K(H_2O)_6)(Al(H_2O)_6)(SO_4)_2$ which implies somewhat more explicitly the association of the univalent and trivalent ions with their respective octohedrons of water molecules.

In 1935 Lipson and Beevers[7] showed that in α type alums the [111] axis of the octohedron of water molecules surrounding an aluminum (R^{3+}) ion coincides with the [111] axis of the crystal, but that the cubic axis of the octohedron are displaced from the cubic axis of the crystal by approximately 9.5° about the [111] direction. The β alums are described as having perfectly regular groups of water molecules with the cubic axes of the octohedron being directed along the cubic axes of the crystal.

The γ alums are said to differ from the α and β alums due to the fact that the sulphate groups of the γ

alums are oriented oppositely along the crystal body diagonals to those of the α and β alums. The cubic axes of the octohedron in the γ alums are rotated about the [111] crystal direction by about 40 degrees. The only known γ alum is the soda alum; $NaAl(SO_4)_2 \cdot 12H_2O$.

The potassium alum used in the author's experiments was an α alum. In the different octants of the unit cell are eight equally dispersed $(SO_4)^{2-}$ groups which consist of a single sulfer surrounded by four tetrahedrally coordinated oxygens.

The crystal field seen by the R^{3+} ion is due to the various surrounding ligands and is dependent upon these ligands' positions and geometric arrangements. The ligands surrounding R^{3+} in order of proximity are:

6 octohedrally coordinated H_2O at 2.0 Å

6 sulfate groups $(SO_4)^{2-}$ at 5.0 Å

6 univalent ions R^{1+} at 6.0 Å

2 sulfate groups $(SO_4)^{2-}$ at 6.5 Å

As indicated in Figure 2 six of the eight sulfate groups form a trigonally distorted octohedron around R^{3+} with the threefold axis of symmetry along a unit cell [111] direction. On this same axis, but outside the octchedron, lie the remaining two sulfate groups at a distance d'_o from R^{3+}. For an alum $d'_o = 0.537a_o$ where a_o is the lattice constant, previously mentioned to be 12.158 Å.

Figure 3 shows the distances and positions of the second and fourth neighbor sulfate ions with respect to the R^{3+} ion. The six second neighbors lie in the $\{110\}$ planes approximately at the intersections of the line through R^{3+}, which forms a 90° angle with the two parallel octant body diagonals. The distance d_o from R^{3+} to each of the octohedron forming sulfates is, for an α alum, $0.407a_o$. Table 1 illustrates the pertinent crystal structure details of the KAl alum used by the author.

Table 1

Alum	Type	a_o	d_o	d_o'
$KAl(SO_4)_2 \cdot 12H_2O$	α	12.158Å	4.948Å	6.529Å

For information on the growth of single crystals of $KAl(SO_4)_2 \cdot 12H_2O$ doped with Ti^{3+} the reader is referred to Appendix A.

CHAPTER IV

EXPERIMENTAL APPARATUS

It is the purpose of this chapter to present a brief description of the electron paramagnetic resonance spectrometer used by the author for the experiments.

4.1 Discussion of the Spectrometer's Components

The spectrometer, manufactured by Varian Corp., is the standard X-Band E.P.R. spectrometer with the optional superhetrodyne accessory included which extends the E.P.R. system operation in many experimental situations by increasing system sensitivity to low modulation frequencies.

The most basic components involved in the spectrometer are:

A) An electromagnet capable of producing fields from zero to approximately 10,000 gauss in the X-Band configuration, with a properly regulated D.C. power supply and with a magnetic field control unit enabling the field to be swept with respect to time about a central field setting.

B) An oscillator in conjunction with modulation coils to produce the low frequency modulation of the main magnetic field H, at the geometrical centre of the gap between the poles of the electromagnet. The modulation frequency used in the author's experiments was 400 Hz.

C) A rectangular sample cavity into which the sample is placed and exposed to the radiated electromagnetic energy originating at the klystron.

D) A signal klystron oscillator which supplies microwave radiation of a constant frequency to the sample cavity at approximately 9.5 GHz.

E) A local klystron oscillator to heterodyne the signal reflected from the cavity at resonance.

F) A crystal detector system.

G) A low temperature Dewar system for experiments performed at liquid nitrogen or liquid helium temperatures.

H) A strip chart recorder for hard copy output.

4.2 Functional Description of Waveguide Network

In this section the actual operation and interconnection of the different components of the spectrometer will be discussed. The first and main

component is the X-Band microwave bridge. A detailed block diagram for this bridge is presented in Figure 6. The microwave bridge consists of a klystron assembly, a hybrid tee, a low and high power arm, and the associated tuning components. The water cooled klystron oscillator generates microwaves over the frequency range of approximately 8.8 to 9.6 GHz. The klystron oscillator is coupled into the waveguide system via a ferrite isolator and a variable attenuator. This ferrite isolator acts on the passage of microwave energy in much the same way as a diode acts on the passage of current in an electrical system. This isolator has a forward attenuation of less than 1 dB and a reverse attenuation of approximately 30 dB, thus essentially eliminating any reflection of power back into the klystron which could alter the frequency of operation of the klystron. The variable attenuator provides adjustable attenuation of the power into the hybrid tee.

After the variable attenuator the power enters the hybrid tee and is divided equally between the low and high power arms of the bridge. When the superheterodyne accessory configuration is utilized, as it was in the author's case, the high power arm is directly coupled to the superheterodyne apparatus and the low power arm is connected to the sample cavity through the cryostat

isolator and the phase shifter. (The cryostat isolator is an adjustable one-way attenuator and allows the incident power on the cavity to be adjusted from -6dB to approximately -40 dB attenuation in reference to the power from the hybrid junction. Since this is a one-way attenuator the signal reflected from the cavity which carries the resonance information passes back through the isolator unattenuated.

As was mentioned above the high power arm of the microwave bridge is directly connected to the X-Band superheterodyne accessory unit. This superheterodyne unit consists of a klystron, known as the local oscillator, ferrite isolator and variable attenuator which perform as they do in the X-Band microwave bridge and were discussed above.

The klystron local oscillator in the superheterodyne unit is tuned to a frequency ± 30 MHz from the original klystron in the microwave bridge. The local oscillator RF power, after passing the isolator and attenuator is coupled into the high power (reference) arm of the microwave bridge through a slidescrew tuner which ensures proper matching between the two units.

Another important component of the spectrometer is the actual sample cavity itself. The cavity is connected to a length of standard (1.27 x 2.54cm.) gold plated brass

waveguide which in turn is connected to the low power arm of the microwave bridge. It is placed inside the helium dewar so that the sample in the cavity rests at the geometric centre and most homogeneous point of the magnet. The cavity resonates in the TE_{102}^{13} rectangular mode. The coupling of the cavity to the microwave guide is variable and may be adjusted from outside the cryostat when working at room or liquid helium temperatures. The reader is referred to Figure 7 for a cross sectional view of the cavity system.

Before discussing the experimental procedure used in order to obtain the E.P.R. spectrum of Ti^{3+} in KAlum it is of interest to first touch upon the topic of the cryostat system used for low temperature experiments. The cryostat used in the author's experiments was a commercially available Andonian Ass. cryostat. The tail of the cryostat is symmetrically placed between the pole faces of the electromagnet. The cryostat contains a length of waveguide to which the cavity is attached and into which the paramagnetic sample is placed. Also contained in the cryostat is a liquid He reservoir, a calibrated germanium thermometer, and a liquid nitrogen reservoir which acts as a radiation shield. The sample is cooled by the flow of liquid He through a surrounding capillary whose quantity may be controlled by an externally connected throttle valve. The temperature of

the sample may be varied and monitored over the range of 1.9° K to 300° K by a temperature-sensing, heating device.[11]

CHAPTER V

EXPERIMENTAL PROCEDURE

5.1 Initial Preparations

In order to prepare the system for liquid Helium temperature experimental runs it was first necessary to properly mount the crystal sample on the bottom horizontal face of the sample cavity. The single crystal of KAl alum had sufficiently well defined crystal faces so that it was a relatively simple procedure to mount the crystal with H parallel to either its {100} plane or {111} plane. Once this was accomplished, the waveguide and attached cavity were suspended within the cryostat so that the sample was at the center of the gap between the dc magnet's pole faces. A preliminary tuning of the klystron was performed at this time in order to check on the cavity dip and thus verify that all was properly operational. It should also be mentioned at this point, that along with the crystal sample in the cavity, was also placed a very small quantity of α, α' - diphenyl - β - picryl hydrazyl (D.P.P.H.)[1] which is a free radical and is the standard klystron frequency determining entity used in the majority of E.P.R. experiments. More will be said later as to how D.P.P.H. is utilized to determine the klystron operating frequency. The next step in the preparatory

procedure was to evacuate and then purge, with dry nitrogen gas, all the reservoirs which during the experiment would contain the cryogenic liquids.[14] Once a good vacuum radiation shield in the outer walls of the cryostat was obtained, by diffusion pumping, it was then possible to fill the secondary chamber with liquid N_2 and let cool for approximately one-half hour. The sample chamber and the helium reservoir were then evacuated and flushed with dry helium gas several times. Liquid He. was then transferred to the cryostat and the temperature of the cavity monitored as it approached 4.2°K.

5.2 Detection of Absorption Points

Once the initial preparations were completed and the temperature of the system stabilized, it was then possible to observe the actual E.P.R. spectrum of the sample. When the frequency of the microwave radiation and the intensity of the magnetic field satisfy the resonance condition of the sample the impedance of the cavity is altered such that a signal is reflected back from the cavity to the crystal diode detector arm of the hybrid tee. At this crystal detector, the reflected signal is heterodyned with the local oscillator frequency. The 30 MHz difference frequency containing

the modulated signal is then passed to the pre-amplifier which is attached to the crystal detector. This signal is then passed through several amplifier units which provide high gain, high sensitivity, noise rejection and sharp response. This signal is then displayed on the strip chart recorder as shown in Figure 8.

[16]

The resonance lines on the chart recorder were displayed as first derivatives of the standard absorption peak. This is explained as in Figure 9. Figure 9 - A represents the change in output at the detector as a function of the steady magnetic field at the sample; Figure 9 - B shows the variation of the field as a function of time when the linear sweep and the sinusoidal field variations are applied; Figure 9 - C shows how the static curve translates these variations into a time varying signal at the output of the microwave detector. The signal at the output of the amplifier varies in time in the manner indicated in Figure 9 - D. The change in the sign of the derivative of the absorption curve is conveyed as in the wave form of Figure 9 - D as a reversal in phase relative to the field modulation waveform. The waveform at the output of the amplifier enters the phase sensitive detector that uses the original sinusoidal waveform as reference. The d.c. output of this detector is a representation of the derivative of the absorption

line as shown in Figure 9 - E.

5.3 Measurement of Magnetic Field Values

In order to determine the value of the magnetic field at the absorption points of the spectrum it was necessary to utilize a Gaussmeter. This method increases the accuracy greatly over the method of taking the magnetic field value directly from the calibrated field control dial. The Gaussmeter utilizes the principle of nuclear magnetic resonance (N.M.R.) and is a commercial unit consisting of a Varian F-9 nuclear Fluxmeter in conjunction with a Hewlett-Packard frequency counter.

Experimentally the magnetic field was determined by sweeping the field partially through the resonance line and then holding it stationary at the crossover point of the first derivative signal. The Gaussmeter probe was then placed between the magnet's pole faces and as close to the sample cavity as possible. After locating the N.M.R. absorption signal on the fluxmeter's oscilloscope the frequency counter assumed a relatively stable value. This value was then multiplied by a constant which was dependent upon the probe used, and the magnetic field value resulted. This method of determining the magnetic field values was repeated for

each line of the various spectra.

5.4 Measurement of the Klystron Operating Frequency

The Gaussmeter was also used in conjunction with the small amount of D.P.P.H. present in the sample cavity in order to determine the klystron operating frequency. The g-factor for D.P.P.H. is known very accurately to be 2.0037 which is very close to the free-electron value of 2.0023. By using the basic resonance equation and accurately determining the magnetic field value for D.P.P.H. at its resonance point the klystron operating frequency was found to be 9.552 GHz. for a particular experiment performed.

CHAPTER VI

CONCLUSION

The electron paramagnetic resonance spectrum of Ti^{3+} doped single crystals of $KAl(SO_4)_2 \cdot 12H_2O$ has been studied by varying the magnetic field in the {100} plane of the crystal.

By using the effective spin Hamiltonian and determining the g_{ij} tensors, the principal g factors were found to be $g_{zz} = 1.979$, $g_{yy} = 1.898$ and $g_{xx} = 1.828$ with an accuracy of ± 0.005. From these results one may conclude that definite anisotropy exists for the principal g values.

These results are in excellent agreement with those obtained by Dionne and MacKinnon, 1968, for Ti^{3+} in $KAl(SO_4)_2 \cdot 12H_2O$ which were $g_{zz} = 1.975$, $g_{xx} = 1.828$ and $g_{yy} = 1.897$.

APPENDIX A

Growth of Single Crystals of Ti^{3+} Doped $KAl(SO_4)_2 \cdot 12H_2O$.

Several problems were encountered when attempts were made to grow single doped crystals of KAl alum. One of the biggest problems was the tendency of Ti^{3+} ions to oxidize in air to the Ti^{4+} state which is a much more stable configuration. This problem was partially overcome by placing the crystal growing solution in an atmosphere of nitrogen. It was possible to detect oxidation by observing the white material which precipitated out of the solution when oxidation occurred. Due to the fact that even in an N_2 atmosphere not all oxidation could be eliminated and some precipitate did form it was necessary to utilize the "Flotation Technique" [9].

This method involves the protection of seed crystals from falling precipitate during the crystal growing process. A cork of approximately 10cm. was floated on the surface of the crystal growing solution in an appropriately sized beaker. Suspended from the underside of the cork was a teflon disc attached to the underside of which were the seed crystals in question. These minute seed crystals were glued to the disc and provided points of nucleation for crystal growth. The benefits of this method were twofold;

first the growing crystals were protected from the precipitate, which could cause defects and secondly the teflon, by its nature, provided very few points of nucleation which greatly increased the chances of obtaining relatively large single crystals with no over-growth of neighboring crystals.

The chemical equation which describes the preparation of the alums is:

$$X_2(SO_4) + 24H_2O + Y_2(SO_4)_3 \longrightarrow 2XY(SO_4)_2 \cdot 12H_2O$$

The proportionate chemical combination of $K_2(SO_4)$ and $Al_2(SO_4)_3$ with water as the activity medium resulted in an aqueous solution of $KAl(SO_4)_2 \cdot 12H_2O$. The solution was then heated and proper amounts of the components were added to obtain a saturated solution at a particular temperature (approx. 80°C). To this was added a small amount of Titanium Trichloride which acted as the source of paramagnetic ions.

The beaker containing the solution and seed crystals was then placed in a circulating bath which provided accurate temperature regulation. The temperature was then able to be controlled so that the solution could be cooled to room temperature over an extended period of time. After many repeated attempts reasonably sized single crystals doped with Ti^{3+} were obtained.

BIBLIOGRAPHY

1.- Al'tshuler, S. A., Kozyrev, B. M., Electron Paramagnetic Resonance. New York: Academic Press, 1963.

2.- Assenheim, H. M., Introduction To Electron Spin Resonance. London: Hilger & Watts Ltd., 1966.

3.- Dionne, G. F., Can. J. Phys., 42, 2419, 1964.

4.- Dionne, G. F., MacKinnon, J. A., Phys. Rev., 172, 325, 1968.

5.- Holden, A., Singer, P., Crystals & Crystal Growing. New York: Anchor Books, 1960.

6.- Lipson, H., Proc. Roy. Soc., 151, 347, 1935.

7.- Lipson, H., Beevers, C. A., Proc. Roy. Soc., A148, 664, 1935.

8.- Low, W., Paramagnetic Resonance In Solids. New York: Academic Press, 1960.

9.- MacKinnon, J. A., Ph. D. Thesis (unpublished) McGill Univ. 1968.

10.- MacKinnon, J. A., Dionne, G. F., Can. J. Phys., 44 2329, 1966.

11.- MacKinnon, J. A., Rev. Sci. Inst., 43, 1847, 1972.

12.- Orton, J. W., An Introduction To Transition Group Ions In Crystals. London: Iliffe Books Ltd., 1968.

13.- Poole, C. P. Jr., Electron Spin Resonance New York: Interscience Publishers, 1967.

14.- Rozenburg, H. M., Low Temperature Solid State Physics. London: Oxford Univ. Press, 1965.

15.- Schlapp, R., Penney, W. G., Phys. Rev. 42, 666, 1932.

16.- Wilmhurst, T. H., Electron Spin Resonance Spectrometers. New York: Plenum Press, 1968.

17.- Wyckoff, R. W. G., Crystal Structures III. New York: Interscience Publishers Inc., 1960.

18.- Van Vleck, J. H., Phys. Rev., 41, 208, 1932.

19.- Zavoisky, E., J. Phys. USSR., 9, 211, 1945.

Table 2

The Angular Variation of the Spectrum in the {100} Plane

	Degrees	Magnetic Field		Degrees	Magnetic Field
(1)	0	3523	(2)	0	3523
	10	3512		10	3546
	20	3513		20	3575
	30	3523		30	3609
	40	3542		40	3642
	50	3568		50	3671
	60	3599		60	3691
	70	3631		70	3700
	80	3659		80	3696
	90	3680		90	3681
	100	3692		100	3655
	110	3692		110	3623
(3)	0	3558	(4)	0	3558
	10	3537		10	3578
	20	3518		20	3595
	30	3501		30	3605
	40	3489		40	3607
	50	3483		50	3600
	60	3484		60	3587

Table 2 (continued)

	Degrees	Magnetic Field		Degrees	Magnetic Field
	70	3492		70	3567
	80	3505		80	3545
	90	3522		90	3523
	100	3542		100	3503
	110	3562		110	3487
(5)	0	3681	(6)	0	3681
	10	3708		10	3645
	20	3725		20	3607
	30	3728		30	3571
	40	3718		40	3542
	50	3695		50	3522
	60	3663		60	3513
	70	3606		70	3517
	80	3590		80	3532
	90	3558		90	3557
	100	3533		100	3591
	110	3519		110	3628

Table 3

The Angular Variation of the Spectrum in the {110} Plane

	Degrees	Magnetic Field		Degrees	Magnetic Field
(1)	0	3523	(2)	0	3523
	10	3499		10	3532
	20	3480		20	3552
	30	3466		30	3579
	40	3460		40	3610
	50	3461		50	3643
	60	3470		60	3672
	70	3486		70	3695
	80	3507		80	3707
	90	3530		90	3707
	100	3554		100	3696
	110	3575		110	3674
(3)	0	3523	(4)	0	3523
	10	3551		10	3527
	20	3577		20	3542
	30	3598		30	3565
	40	3609		40	3595
	50	3611		50	3627
	60	3602		60	3658
	70	3584		70	3684

Table 3 (continued)

	Degrees	Magnetic Field		Degrees	Magnetic Field
	80	3559		80	3701
	90	3530		90	3707
	100	3502		100	3702
	110	3478		110	3685
(5)	0	3558	(6)	0	3558
	10	3524		10	3567
	20	3494		20	3581
	30	3433		30	3598
	40	3461		40	3617
	50	3461		50	3634
	60	3471		60	3649
	70	3492		70	3658
	80	3521		80	3661
	90	3554		90	3657
	100	3589		100	3648
	110	3621		110	3633
(7)	0	3558	(8)	0	3558
	10	3555		10	3593
	20	3559		20	3626
	30	3568		30	3650
	40	3582		40	3663

Table 3 (continued)

	Degrees	Magnetic Field		Degrees	Magnetic Field
	50	3599		50	3662
	60	3617		60	3648
	70	3635		70	3623
	80	3649		80	3590
	90	3657		90	3554
	100	3660		100	3520
	110	3656		110	3502
(9)	0	3681	(10)	0	3681
	10	3711		10	3689
	20	3726		20	3691
	30	3722		30	3687
	40	3699		40	3678
	50	3663		50	3665
	60	3617		60	3648
	70	3568		70	3632
	80	3523		80	3617
	90	3485		90	3604
	100	3460		100	3597
	110	3448		110	3595

Table 3 (continued)

	Degrees	Magnetic Field		Degrees	Magnetic Field
(II)	0	3681	(I2)	0	3681
	10	3670		10	3640
	20	3656		20	3594
	30	3641		30	3547
	40	3626		40	3506
	50	3613		50	3475
	60	3603		60	3456
	70	3599		70	3452
	80	3599		80	[illegible]62
	90	3604		90	[illegible]85
	100	3614		100	[illegible]21
	110	3628		110	3564

Table 4

The Angular Variation of the Spectrum in the {III} Plane

	Degrees	Magnetic Field		Degrees	Magnetic Field
(1)	0	3632	(2)	0	3457
	10	3603		10	3453
	20	3568		20	3460
	30	3534		30	3479
	40	3502		40	3506
	50	3478		50	3540
	60	3464		60	3576
	70	3460		70	3611
	80	3467		80	3639
	90	3485		90	3657
	100	3512		100	3663
	110	3545		110	3654
(3)	0	3525	(4)	0	3566
	10	3523		10	3579
	20	3526		20	3590
	30	3534		30	3597
	40	3545		40	3600
	50	3559		50	3597
	60	3573		60	3591

Table 4 (continued)

	Degrees	Magnetic Field		Degrees	Magnetic Field
	70	3587		70	3581
	80	3598		80	3568
	90	3604		90	3554
	100	3606		100	3542
	110	3603		110	3532
(5)	0	3573	(6)	0	3588
	10	3601		10	3574
	20	3629		20	3558
	30	3645		30	3543
	40	3649		40	3530
	50	3641		50	3520
	60	3622		60	3515
	70	3595		70	3515
	80	3563		80	3520
	90	3530		90	3530
	100	3502		100	3544
	110	3479		110	3559
(7)	0	3598	(8)	0	3599
	10	3609		10	3553
	20	3625		20	3511
	30	3645		30	3479

Table 4 (continued)

	Degrees	Magnetic Field		Degrees	Magnetic Field
	40	3666		40	3458
	50	3685		50	3451
	60	3701		60	3458
	70	3710		70	3480
	80	3713		80	3513
	90	3707		90	3554
	100	3696		100	3600
	110	3678		110	3645
(9)	0	3632	(10)	0	3649
	10	3603		10	3627
	20	3568		20	3609
	30	3534		30	3597
	40	3502		40	3591
	50	3478		50	3592
	60	3464		60	3601
	70	3460		70	3616
	80	3467		80	3635
	90	3485		90	3657
	100	3512		100	3670
	110	3545		110	3698

Table 4 (continued)

	Degrees	Magnetic Field		Degrees	Magnetic Field
(II)	0	3683	(I2)	0	3712
	I0	3709		I0	3719
	20	3719		20	3719
	30	3711		30	3711
	40	3687		40	3697
	50	3650		50	3678
	60	3606		60	3656
	70	3560		70	3636
	80	3519		80	3618
	90	3485		90	3604
	I00	3464		I00	3598
	II0	3456		II0	3598

Table 5

The Orientations of the I2 g_{ij} Tensors

Magnetic Complex	Direction Cosine	g_{zz}	g_{xx}	g_{yy}
		I.979	I.828	I.898
I	cos α	-0.68	-0.07	-0.72
	cos β	-0.37	-0.89	0.26
	cos γ	-0.63	0.44	0.64
2	cos α	-0.68	0.07	0.72
	cos β	-0.37	-0.89	-0.26
	cos γ	0.63	-0.44	0.64
3	cos α	0.68	-0.07	0.72
	cos β	-0.37	-0.89	0.26
	cos γ	-0.63	0.44	0.64
4	cos α	-0.68	-0.07	0.72
	cos β	0.37	-0.89	0.26
	cos γ	-0.63	-0.44	-0.64
5	cos α	-0.63	0.44	0.64
	cos β	-0.68	0.07	-0.72
	cos γ	-0.37	-0.89	0.26

Table 5 (continued)

Magnetic Complex	Direction Cosine	g_{zz}	g_{xx}	g_{yy}
		I.979	I.828	I.898
6	cos α	-0.63	-0.44	-0.64
	cos β	-0.68	-0.07	0.72
	cos γ	0.37	-0.89	0.26
7	cos α	-0.63	0.44	0.64
	cos β	0.68	-0.07	0.72
	cos γ	-0.37	-0.89	0.26
8	cos α	0.63	-0.44	0.64
	cos β	-0.68	0.07	0.72
	cos γ	-0.37	-0.89	-0.26
9	cos α	0.37	-0.89	0.26
	cos β	-0.63	-0.44	-0.64
	cos γ	-0.68	-0.07	0.72
IO	cos α	-0.37	-0.89	-0.26
	cos β	0.63	-0.44	0.64
	cos γ	-0.68	0.07	0.72

Table 5 (continued)

Magnetic Complex	Direction Cosine	g_{zz}	g_{xx}	g_{yy}
		I.979	I.828	I.898
II	cos α	-0.37	-0.89	0.26
	cos β	-0.63	0.44	0.64
	cos γ	0.68	-0.07	0.72
I2	cos α	-0.37	-0.89	0.26
	cos β	-0.37	0.44	0.64
	cos γ	-0.68	0.07	-0.72

α, β, γ are referred to the crystallographic axes.

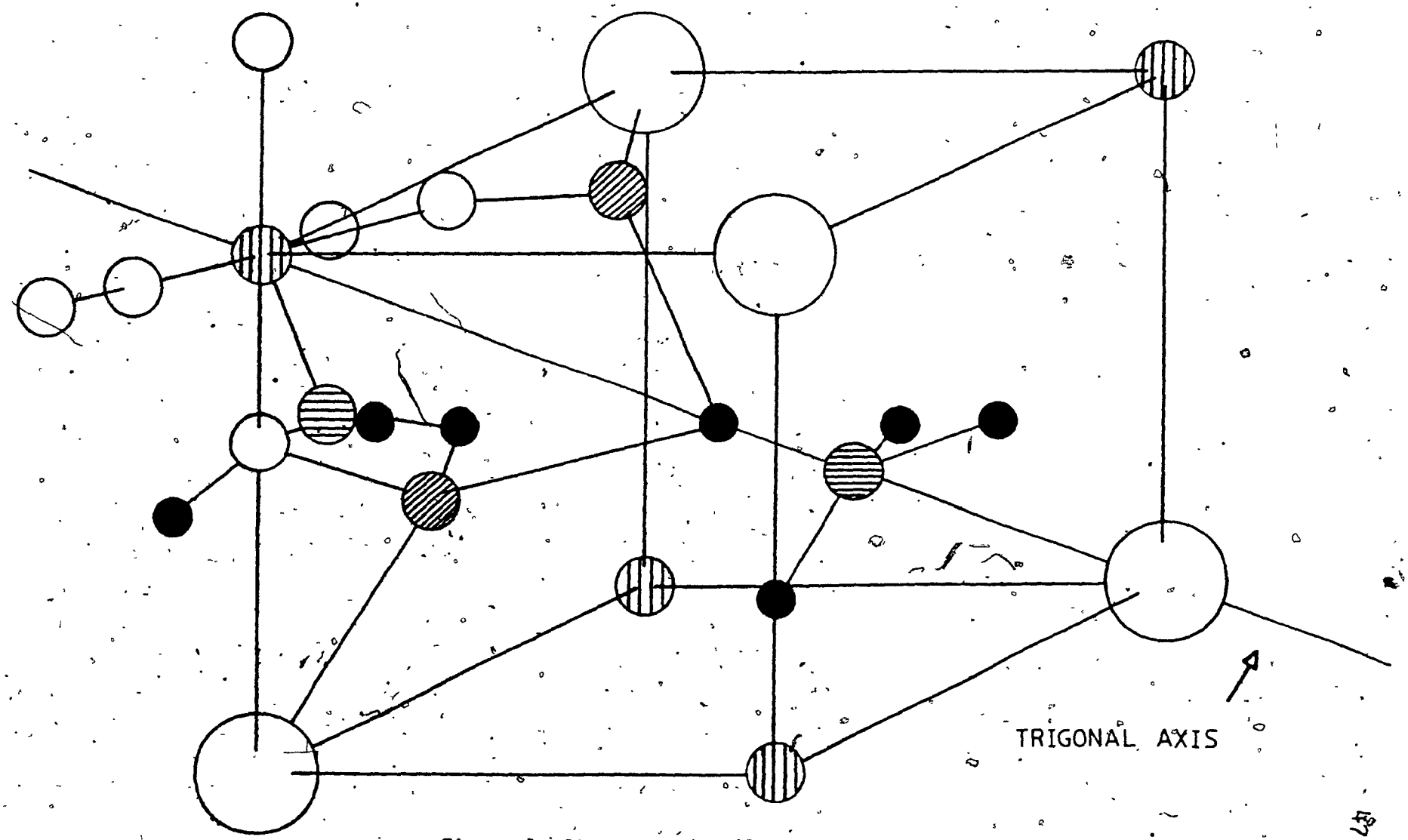

Figure 1 Structure details of one octant of KAl Alum.

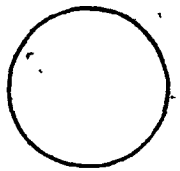

R^{1+} = MONOVALENT ION = POTASSIUM

R^{3+} = TRIVALENT ION = ALUMINUM

S = SULFUR

H_2O = WATER

O = OXYGEN

Legend to Figure 1.

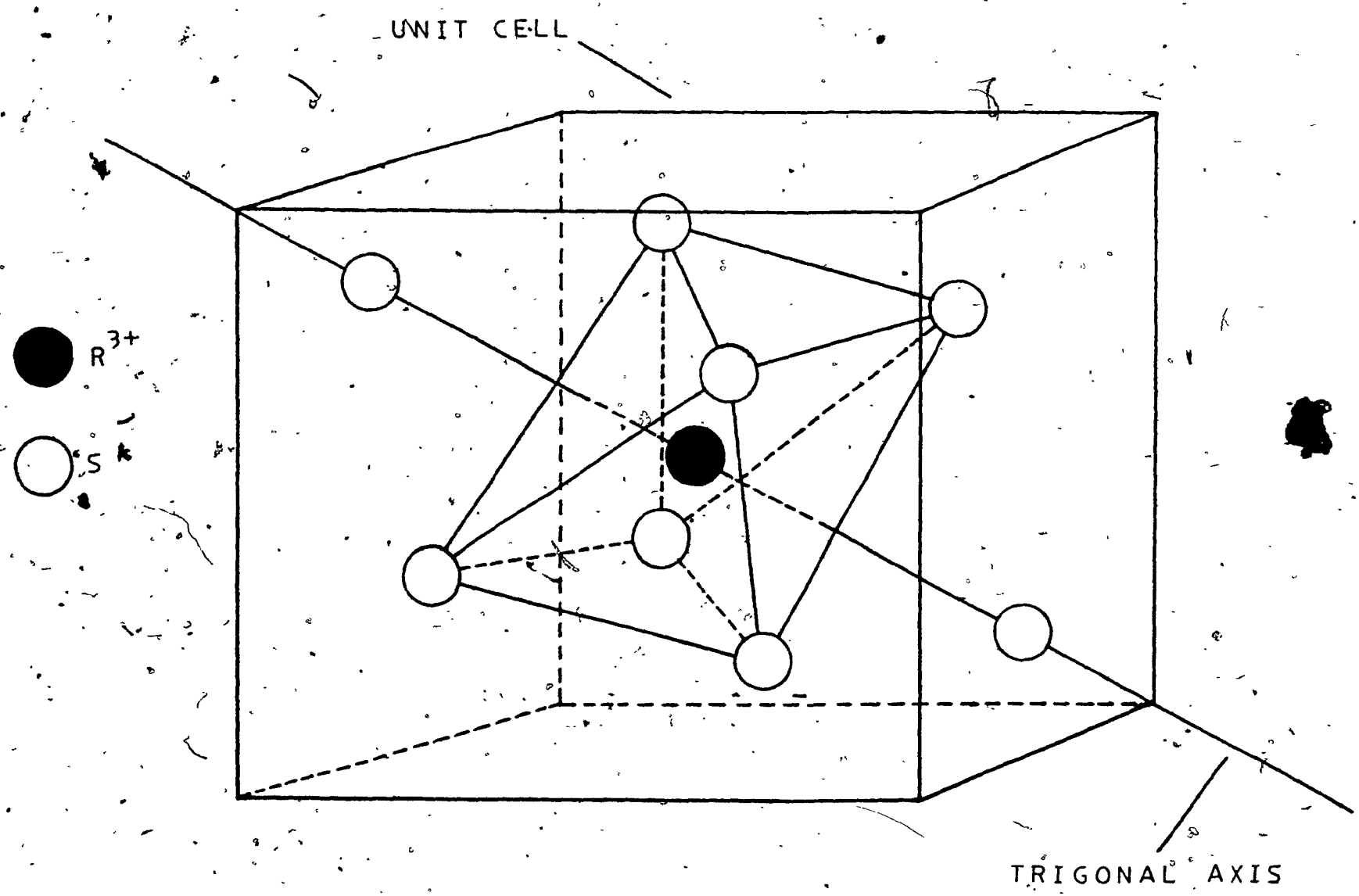

Figure 2 Trigonally distorted octohedron formed by second neighbor Sulfur atoms

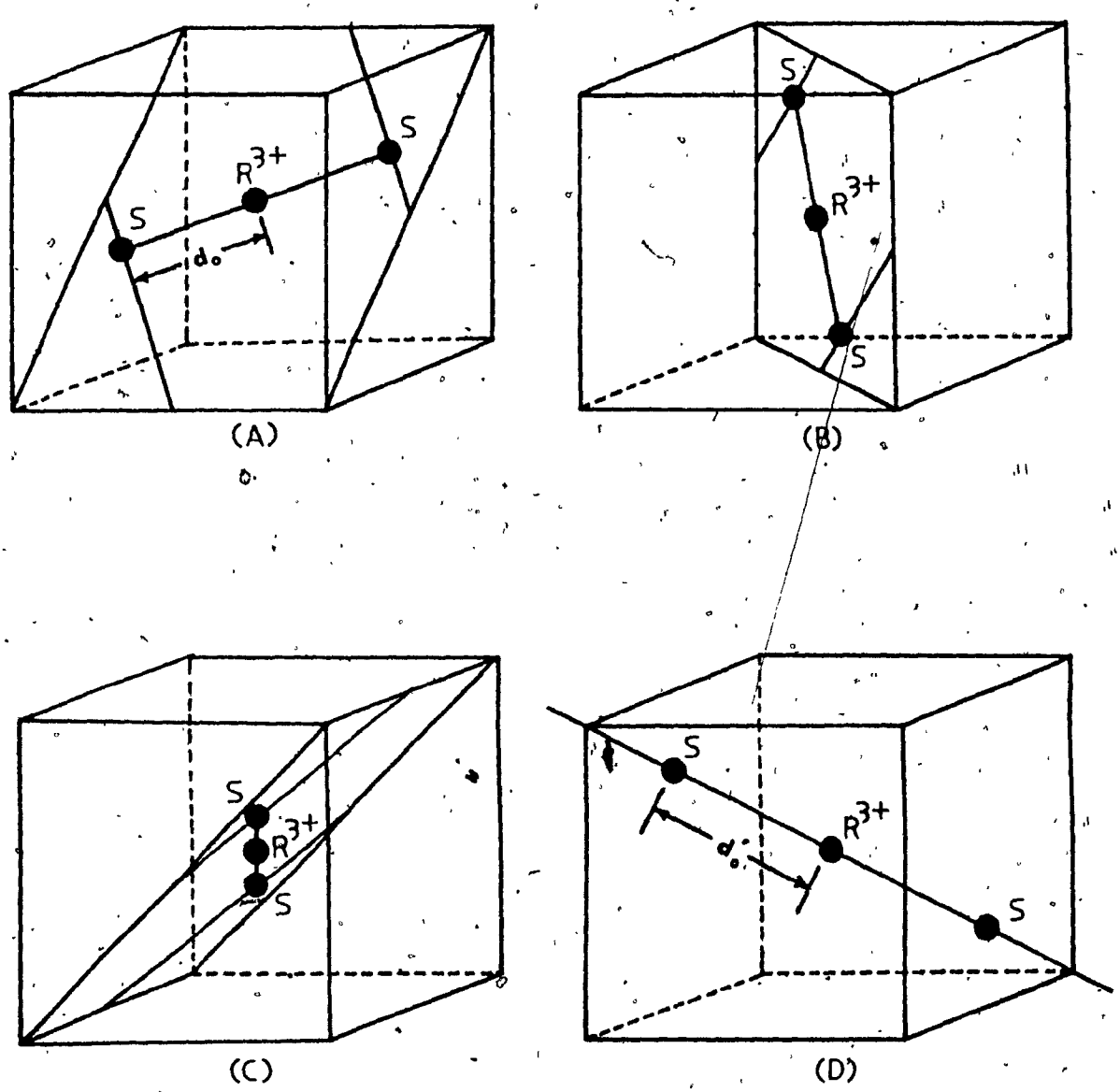

Figure 3. The locations of the eight sulfur atoms which surround R^{3+} in a unit cell are shown schematically. In (a) through (c), the three pairs of second-neighbor sulfurs are presented as lying in {110} planes at the intersections of [111] axes in their respective octants and the line approximately perpendicular to these axes passing through R^{3+} at the center of the unit cell. The distance from R^{3+} to each of these six S atoms is denoted by d_o. In (d), the two fourth-neighbor sulfurs are shown as lying on the main body diagonal at a distance from R^{3+} denoted by d'_o.

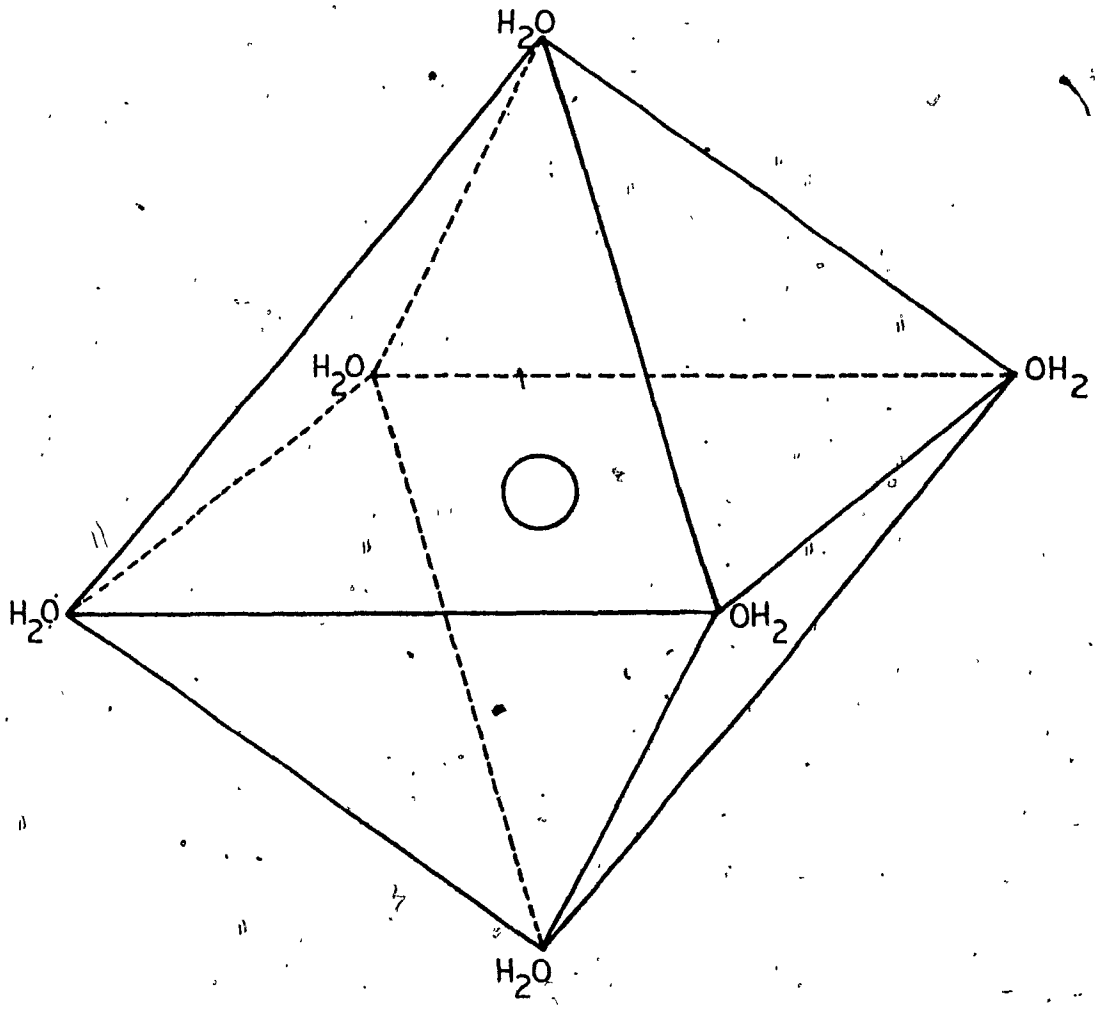

Figure 4 Octohedron of water molecules surrounding a paramagnetic ion.

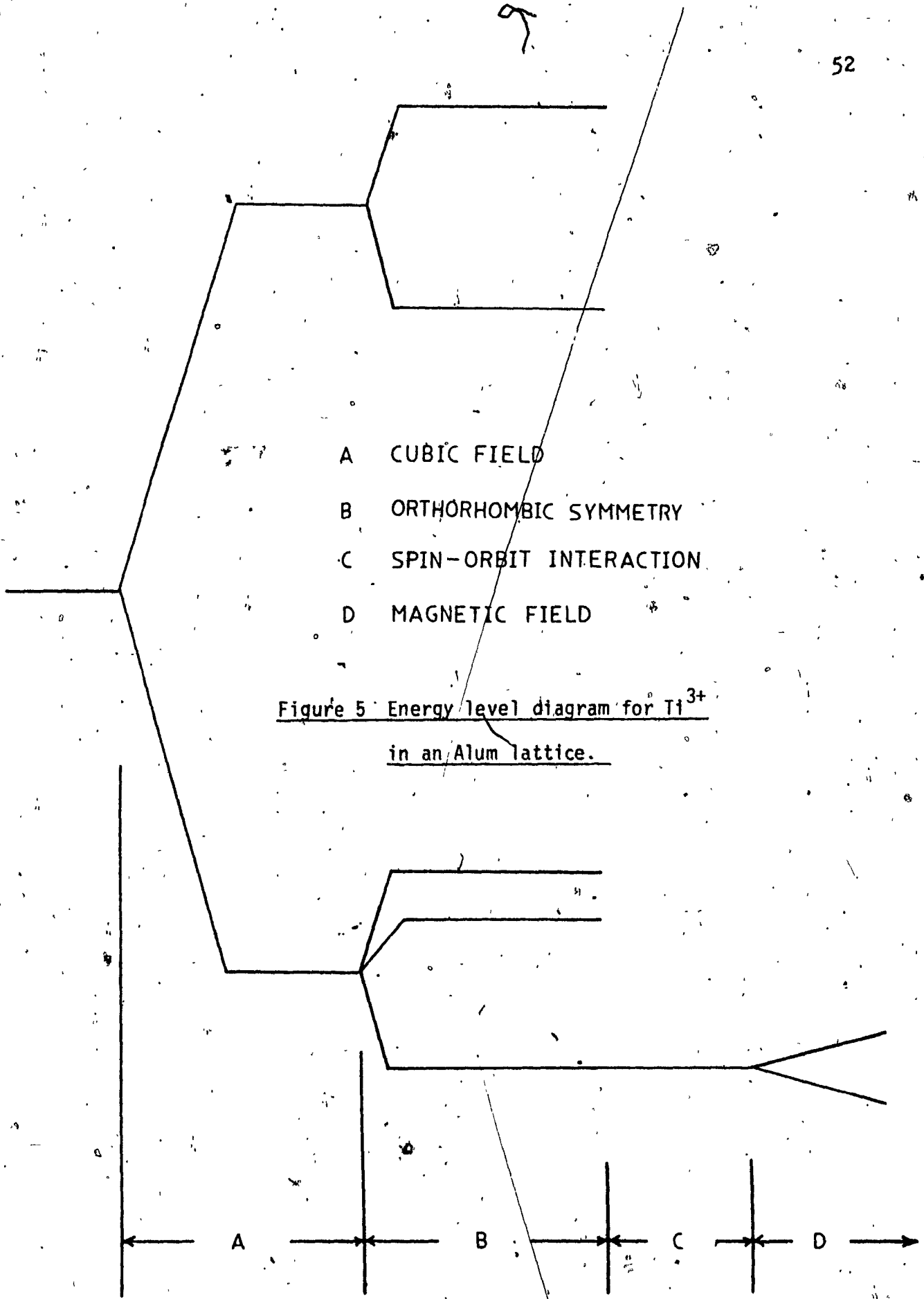

Figure 5 Energy level diagram for Ti^{3+} in an Alum lattice.

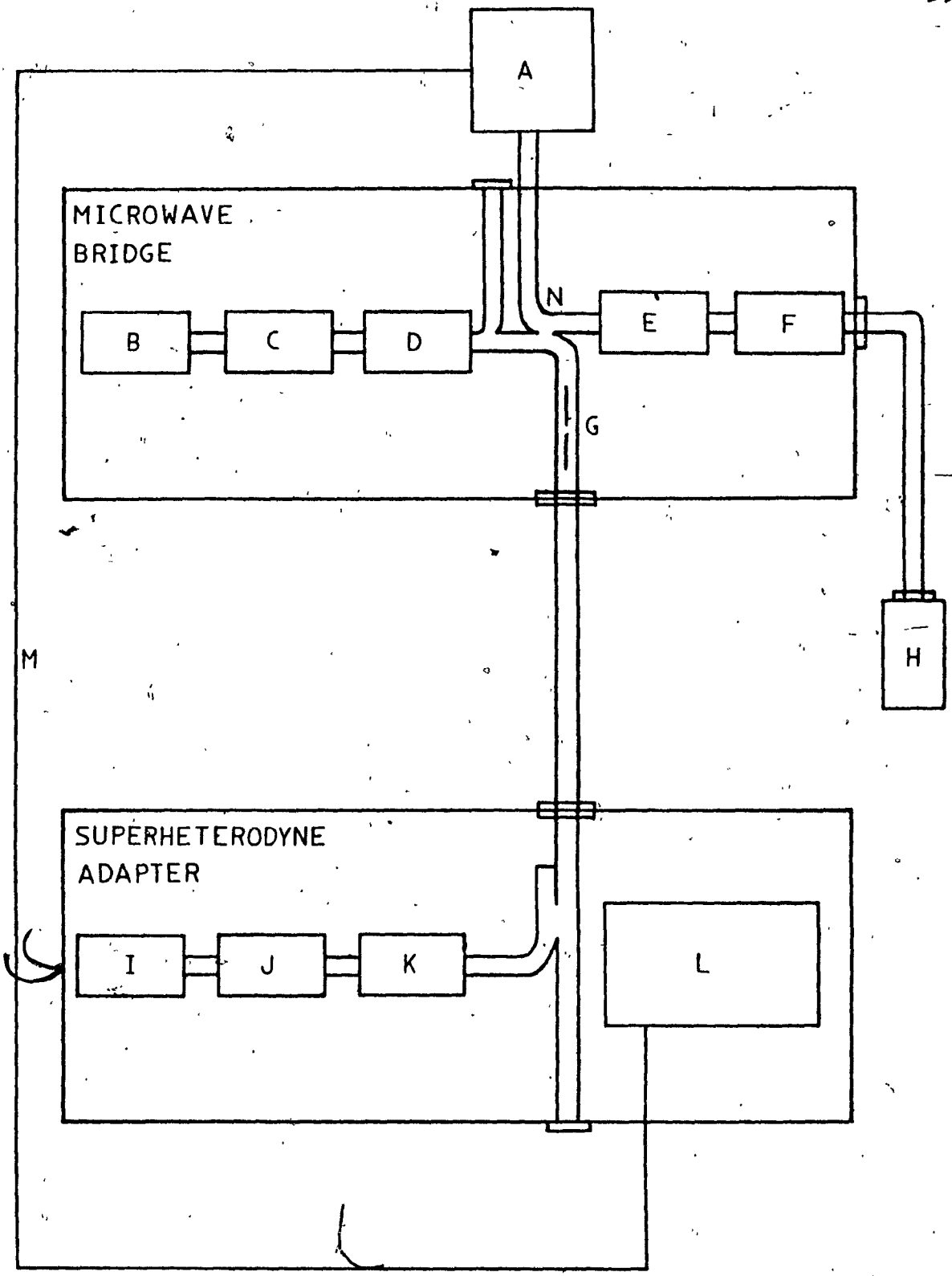

Figure 6. Block diagram of the microwave bridge and superheterodyne adaptor.

Legend to Figure 6

A - Pre-amplifier and detector

B - Main klystron

C - Ferrite isolator

D - Variable attenuator

E - Cryostat isolator

F - Phase shifter

G - Slidescrew tuner

H - Sample cavity

I - Local oscillator klystron

J - Ferrite isolator

K - Variable attenuator

L - 30 MHz IF amplifier and second detector

M - RF cable

N - Hybrid junction

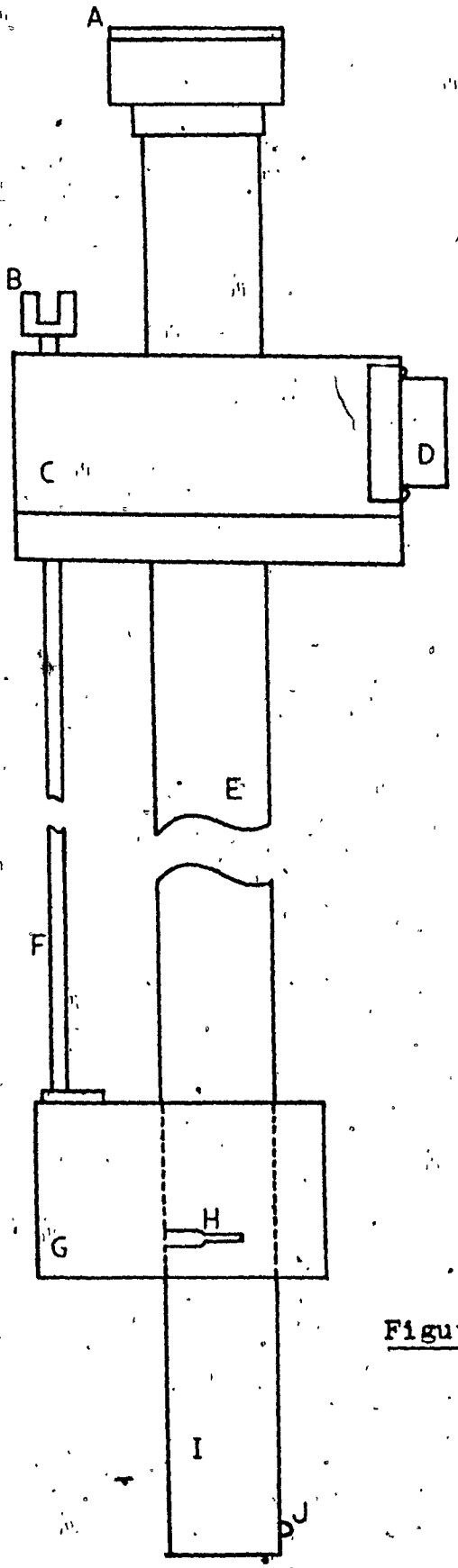

Figure 7. Cross sectional view of the cavity.

Legend to Figure 7

A - Mica plate and waveguide connector

B - External coupling pin control

C- Knurled cryostat plug

D - Temperature control device connectors

E - Connecting length of waveguide

F - Coupling pin connector shaft

G - Gearbox housing for coupling pin control

H - Coupling pin

I - Sample cavity

J - Platinum, germanium resistance sensor : thermometer (MacKinnon, J.A., 1972)

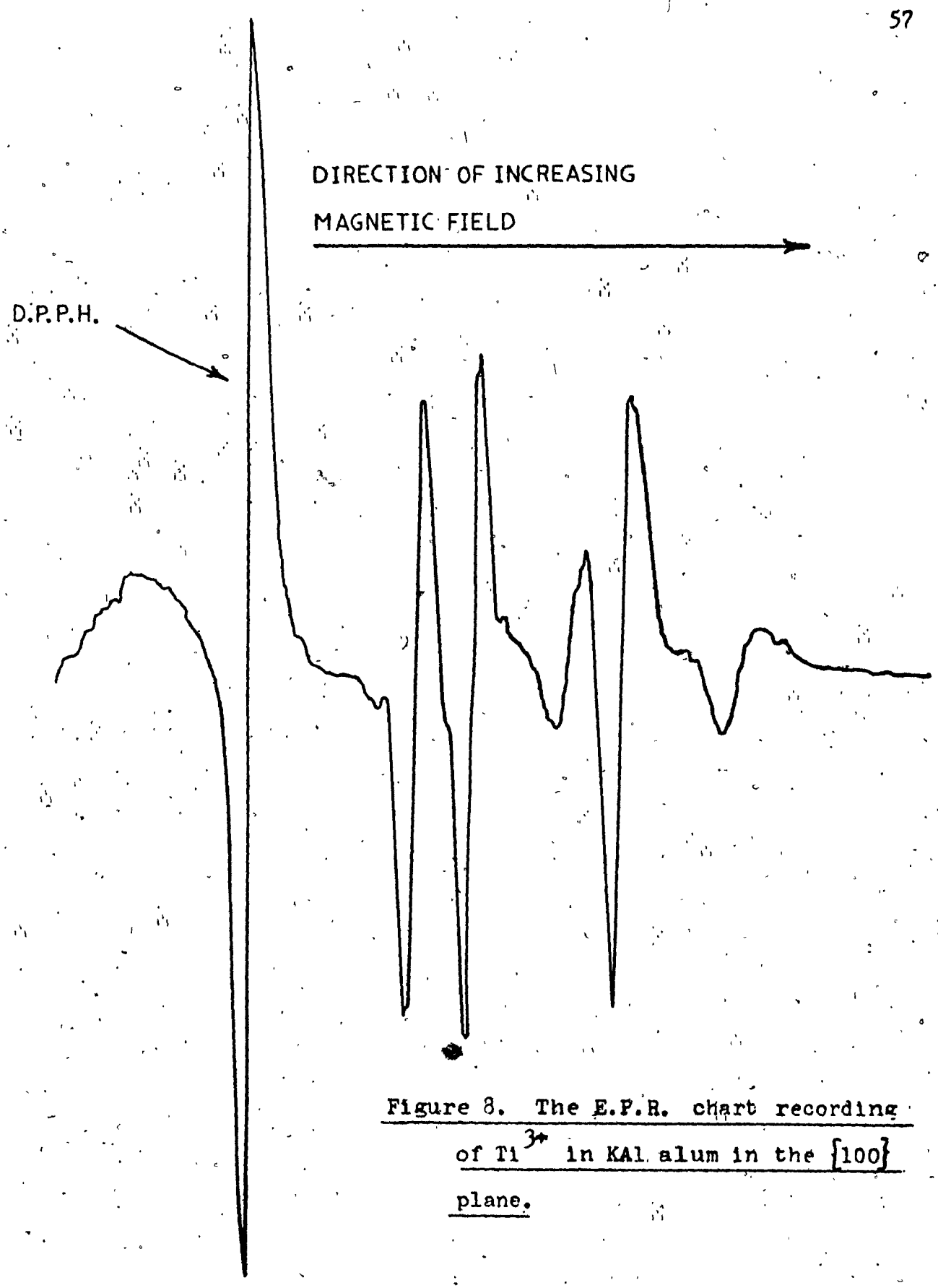

Figure 8. The E.P.R. chart recording of Ti^{3+} in KAl alum in the {100} plane.

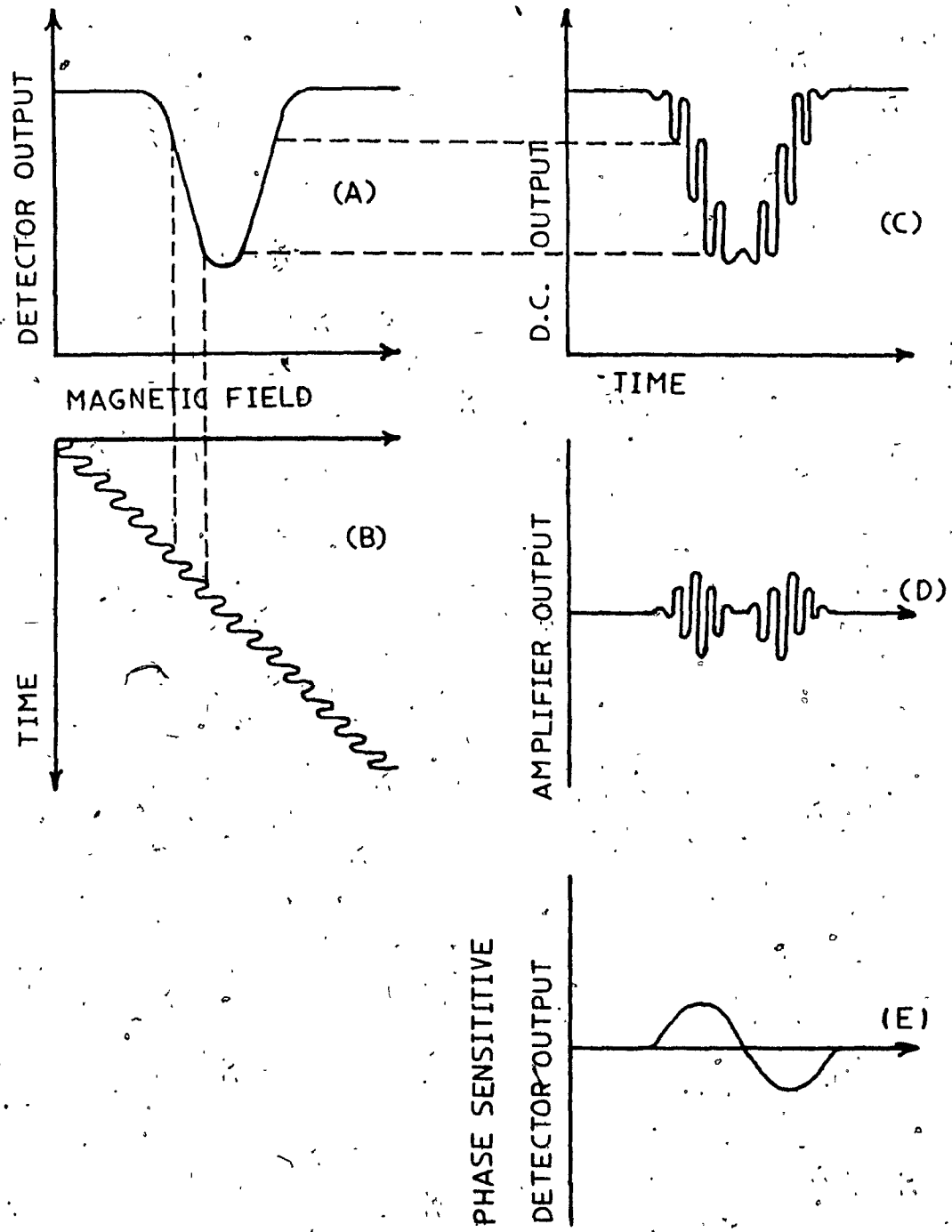

Figure 9. Illustration of first derivative output for absorption points.

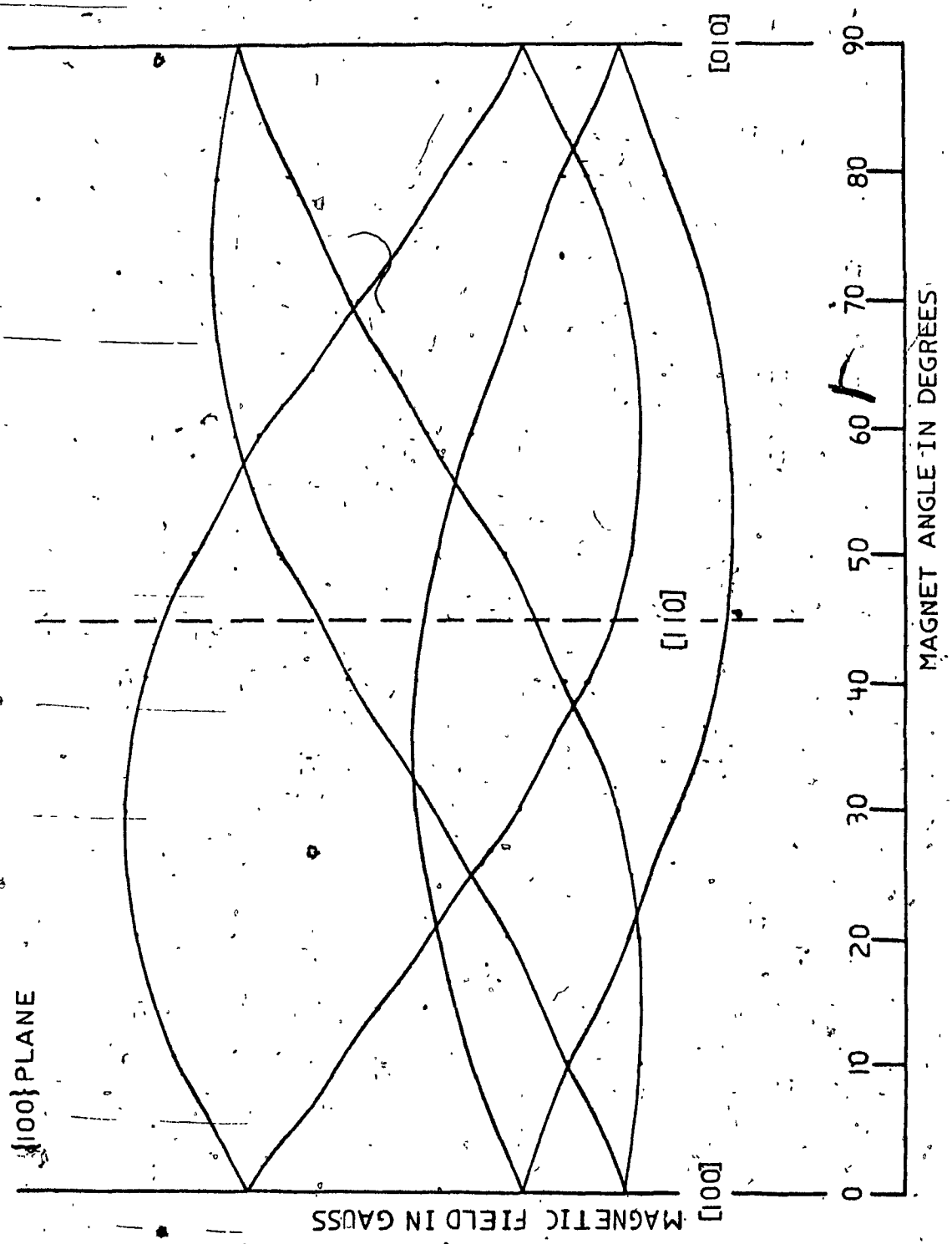
{100} PLANE
MAGNETIC FIELD IN GAUSS
[001]
[011]
[010]
0
10
20
30
40
50
60
70
80
90
MAGNET ANGLE IN DEGREES

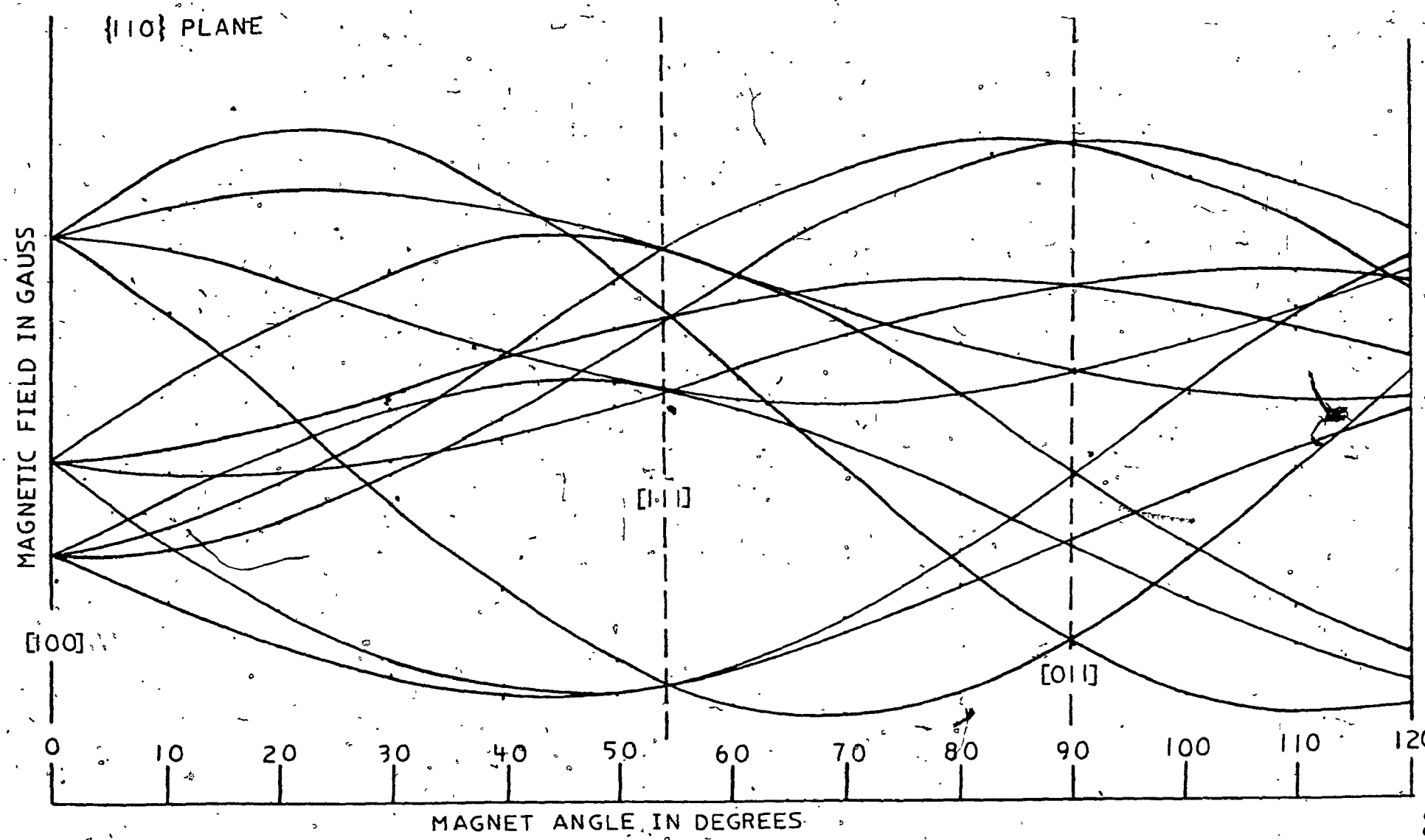
{110} PLANE
MAGNETIC FIELD IN GAUSS
[100]
[1-11]
[011]
0
10
20
30
40
50
60
70
80
90
100
110
120
MAGNET ANGLE IN DEGREES

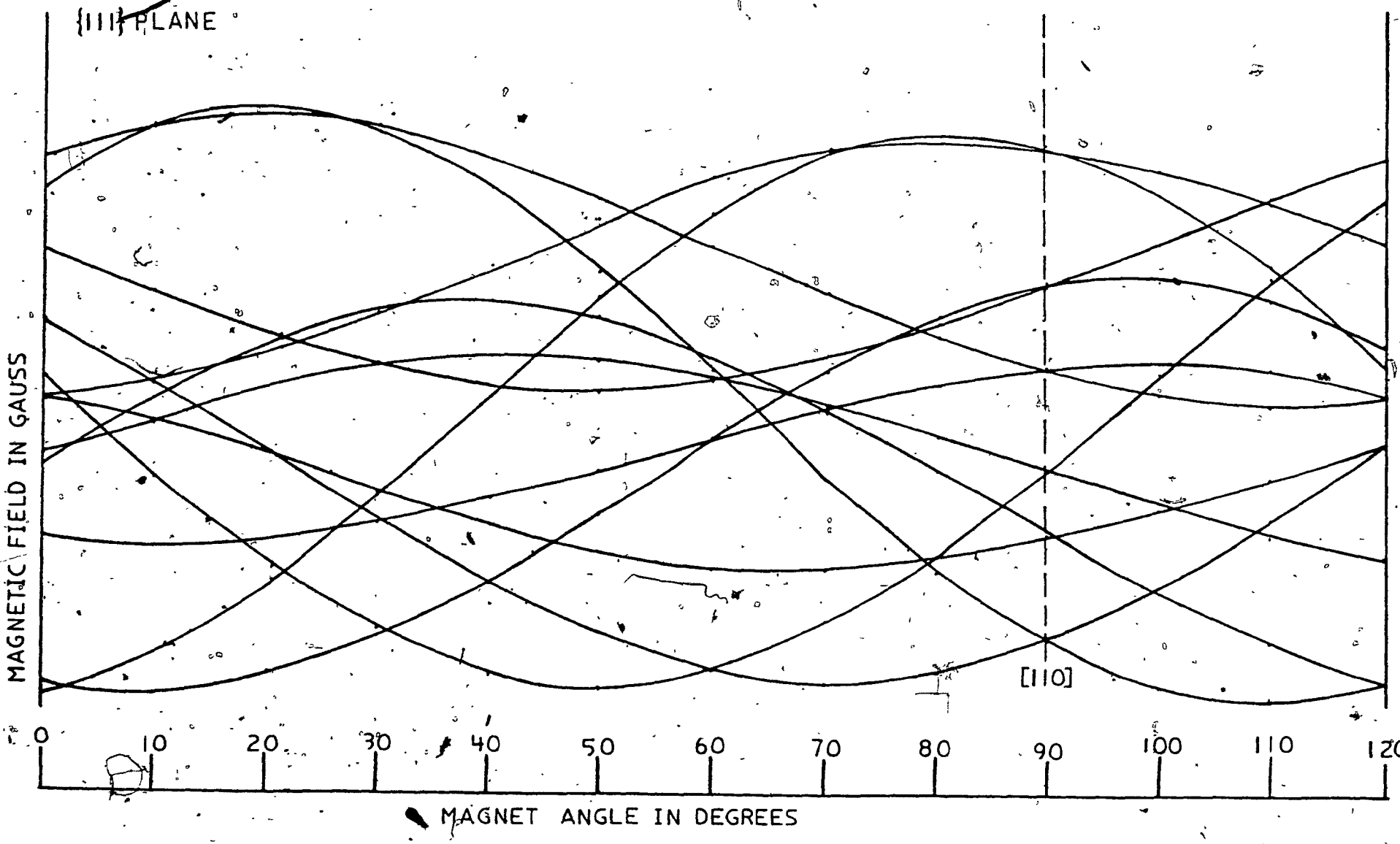
{111} PLANE
MAGNETIC FIELD IN GAUSS
[110]
0
10
20
30
40
50
60
70
80
90
100
110
120
MAGNET ANGLE IN DEGREES